physics

MDPI

Article

Controlling Magnetic Energy Confinement in One- and Three-Dimensional Systems

José Holanda [1,2,3,4,5]

[1] Programa de Pós-Graduação em Engenharia Física, Universidade Federal Rural de Pernambuco, Cabo de Santo Agostinho 54518-430, Pernambuco, Brazil; joseholanda.silvajunior@ufrpe.br
[2] Group of Optoelectronics and Spintronics, Universidade Federal Rural de Pernambuco, Cabo de Santo Agostinho 54518-430, Pernambuco, Brazil
[3] Unidade Acadêmica do Cabo de Santo Agostinho, Universidade Federal Rural de Pernambuco, Cabo de Santo Agostinho 54518-430, Pernambuco, Brazil
[4] Programa de Pós-Graduação em Física Aplicada, Universidade Federal Rural de Pernambuco, Recife 52171-900, Pernambuco, Brazil
[5] Programa de Pós Graduação em Tecnologias Energéticas e Nucleares (Proten), Universidade Federal de Pernambuco, Recife 50740-545, Pernambuco, Brazil

Abstract

This paper investigates the control of magnetic energy confinement in one- and three-dimensional magnetic systems by systematically accounting for magnetic interactions. The analysis provides new insight into magnetic behavior at the nanoscale and introduces a simulation-based framework that clearly distinguishes between magnetizing and demagnetizing interaction regimes. Within this framework, magnetic energy confinement is rigorously defined and can be quantitatively controlled through the underlying interaction landscape. To validate this approach, extensive numerical simulations were performed on representative one- and three-dimensional nanostructures, including individual nanowires and hexagonal arrays of nanowires. Each nanowire was modeled as a chain of interacting ellipsoidal grains, enabling an accurate description of the complex magnetic interactions governing energy confinement in these systems.

Keywords: magnetic energy confinement; magnetic interactions; nanowires; magneticenergy; hexagonal arrays of nanowires

1. Introduction

Recent investigations underscore the growing significance of controlling the size, shape, and orientation of one-dimensional magnetic nanostructures, particularly nanowires [1–8]. These magnetic nanostructures have garnered significant attention due to their transformative applications in advanced spintronics [9], cutting-edge sensor devices, and innovative biomedical technologies [7,10]. They represent a crucial research frontier for exploring diverse magnetic phenomena, including magnetization reversal and complex magneto-optical processes [1–10]. The pursuit of tunable magnetic interactions through novel methodologies promises to yield groundbreaking advancements in this field. The fabrication of nanostructures with well-defined dimensions benefits greatly from template-assisted growth techniques. Notably, the electrochemical synthesis of metallic magnetic nanowires has emerged as a highly effective approach for producing nanoscale systems [11–18]. Electrodeposition within alumina membranes stands out as the most prevalent method for fabricating these systems, resulting in highly ordered arrays of magnetic nanowires embedded within the membrane pores [11–15]. Noteworthy studies report

Check for updates

Received: 22 January 2026
Revised: 8 February 2026
Accepted: 27 February 2026
Published: 3 April 2026

Copyright: © 2026 by the author. Licensee MDPI, Basel, Switzerland. This article is an open access article distributed under the terms and conditions of the Creative Commons Attribution (CC BY) license.

the presence of various magnetization reversal modes, with the coherent configuration often dominating [1–16].

Understanding the effects of magnetic interactions in particulate media is critical, as these interactions can profoundly influence the magnetic properties of nanostructures [19–23]. In general, the magnetization induced by an applied magnetic field comprises both reversible and irreversible components. This complexity makes it impossible to disentangle these components from a hysteresis curve, a finding widely acknowledged in the field. As a result, much vital information remains concealed, leading to a limited understanding of remanent properties. The investigation of the remanent state serves as a powerful tool for probing magnetic interactions. In specific systems, established delta-m (Δm) curves (the change in magnetization) provide compelling insights, allowing meaningful comparisons between isothermal remanent magnetization (IRM) and direct current demagnetization (DCD) data [19,24–29].

In an IRM(H) experiment, where H stands for the applied magnetic field, the investigation begins with a demagnetized sample that has been cooled in zero magnetic field,. Once the desired temperature is reached, a small magnetic field is applied, allowing sufficient time for the system to reach thermodynamic equilibrium. After the magnetic field is removed, the remanence is measured. This procedure is repeated with progressively increasing magnetic field strength until the sample reaches saturation, at which point the remanence attains its maximum value. In contrast, the DCD(H) experiment begins with the sample in a saturated state. At a fixed temperature, the applied magnetic field is gradually reversed until it reaches a small value opposing the initial magnetization. The magnetic field is then switched off, and the remanence is measured. This cycle is repeated with increasing reversed magnetic field strength until saturation is achieved. Through these carefully designed procedures, one can qualitatively assess the dominant type of magnetic interactions—magnetizing or demagnetizing—present in magnetic samples [19,24–33]. In the absence of such interactions, the magnetic system follows the Stoner–Wohlfarth model [19,29].

This study presents a novel approach to accurately determine the intensity of the dominant magnetic interactions in nanostructures. Furthermore, a comprehensive numerical analysis is conducted to investigate how the intensity of these magnetic interactions varies with the angle of the applied magnetic field. These results elucidate the behavior of magnetic interactions as a function of their intensity, revealing two distinct states: magnetizing and demagnetizing. This research enhances the understanding of magnetic interactions in nanostructures and paves the way for advances in applications that exploit these fundamental principles.

2. Approach for the Numerical Calculations

The interactions within magnetic nanostructures have been qualitatively examined using Δm curves [19,24–29]. These Δm curves provide a critical comparison between IRM(H) and DCD(H). Both IRM(H) and DCD(H) are measured using identical experimental methodologies, differing only in the magnetic state of the sample at the beginning of each measurement [15]. The approach presented here is valid in the regime where the anisotropy energy barrier satisfies $K_{eff}V >> k_BT$ [15,19,29] (with K_{eff} the effective magnetic anisotropy constant, V the volume of the material, T the temperature, and k_B the Boltzmann constant), such that thermal activation (Arrhenius–Néel relaxation) does not significantly affect magnetization reversal during the measurement timescale. In other words, the effective magnetic energy is much greater than the Boltzmann energy. The foundational paper by Edmund Stoner and Erich Wohlfarth established [19,29] an underlying relationship between IRM(H) and DCD(H) for non-interacting particles expressed as follows:

$$m_{d1} = 1 - 2m_r, \tag{1}$$

where the variables $m_{d1} = DCD(H)_1/IRM(H_{Max})$ and $m_r = IRM(H)/IRM(H_{Max})$ correspond to specific magnetic characteristics of the material. In contrast, Henkel's theory ($m_d(H) \times m_r(H)$) states that any deviation from the relationship (1) in real systems arises from interactions between nanoparticles [24–28]. This interpretation of Henkel curves highlights that, when magnetic interactions are present, experimental data inherently deviate from the predictions of the Stoner–Wohlfarth equation. This deviation is significant, as the original equation assumes equivalence between magnetizing and demagnetizing processes. To accurately assess the nature of these interactions, a key term, delta-m (Δm), is introduced within the framework of the original equation [24–28]. The interpretation of Δm is given by

$$m_{d2}(H) = \Delta m + [1 - 2m_r(H)], \tag{2}$$

where $m_{d2} = DCD(H)_2/IRM(H_{Max})$. Now, if $\Delta m < 0$, the predominant interactions are demagnetizing (PID); conversely, if $\Delta m > 0$, the predominant interactions are magnetizing (PIM). Understanding these interactions is not merely an academic exercise but is fundamentally important for advancing the field. The underlying premise is that the area defined by these equations serves as a quantitative measure of the strength of magnetic interactions and is therefore highly relevant for experimental and numerical analyses. By employing Riemann sums to reformulate the original Equations (1) and (2), a more robust description of magnetic interactions in these nanostructures can be obtained:

$$I_1 = \lim_{\|\delta\| \to 0} \sum_{i=1}^{N} m_{d1}^i \delta_i m_r. \tag{3}$$

Using Equation (2), the following expression is obtained:

$$I_2 = \lim_{\|\delta\| \to 0} \sum_{i=1}^{N} m_{d2}^i \delta_i m_r, \tag{4}$$

where $\|\delta\| = Max\{\delta_i m_r, 1 \leq i \leq N\}$. and N denotes the number of magnetic interactions. The intensity of the magnetic interactions is then determined from the expressions (3) and (4) as follows:

$$I = \lim_{\|\delta\| \to 0} \sum_{i=1}^{N} \left| m_{d2}^i - m_{d1}^i \right| \delta_i m_r = \lim_{\|\delta\| \to 0} \sum_{i=1}^{N} |\Delta m_i| \delta_i m_r, \tag{5}$$

with m_r defined within the interval $\left[m_r^{in}, m_r^{fi}\right]$. Since the expression (5) can describe both PID and PIM interactions, the following relationships apply:

$$I = \lim_{\|\delta\| \to 0} \sum_{i=1}^{N} |\Delta m_i| \delta_i m_r \rightarrow \begin{cases} \Delta m_i < 0 \text{ for PID,} \\ \Delta m_i > 0 \text{ for PIM.} \end{cases} \tag{6}$$

3. Results and Discussion

The numerical results obtained using this approach focus on two distinct nanostructures in different dimensionalities: (a) a one-dimensional (1D) system consisting of a single nanowire, and (b) a three-dimensional (3D) system comprising a hexagonal array of nanowires. Each nanowire is represented as a chain of interacting ellipsoidal grains, capturing the complex interactions inherent to these low-dimensional systems. The approach developed in this study to be understood as an effective analytical framework whose validity is restricted to a well-defined physical regime. It assumes that the magnetic elements behave as single-domain particles, that magnetization reversal within each grain occurs via coherent rotation, and that dipolar interactions constitute the dominant long-range

coupling mechanism between neighboring elements. Intra-grain exchange is implicitly responsible for maintaining uniform magnetization within each particle, while inter-grain exchange, when present, is treated as a short-range or effective mean-field contribution. Under these conditions, typically satisfied in high-aspect-ratio nanowires with sufficiently small grain size and moderate thermal activation, the reduced energy-based description provides a consistent and computationally tractable approach for quantifying magnetizing and demagnetizing interaction intensities. All numerical calculations have been performed in Python 3.11.0.

3.1. 1D: Featuring a Single Nanowire

Figure 1a presents an expression for the magnetic energy density in the presence of an applied magnetic field, as reported in Refs. [2,15]. This relationship highlights the significant influence of external fields on the nanowire (NW) energy landscape:

$$E_{NW} = \pi M_{Max}^2 \left[\left(\frac{3V_e k_n}{\pi r^3} \right) + (1 - 3N_{//}) \right] \sin^2(\varphi + \theta_H) - M_{Max} H \cos\varphi. \quad (7)$$

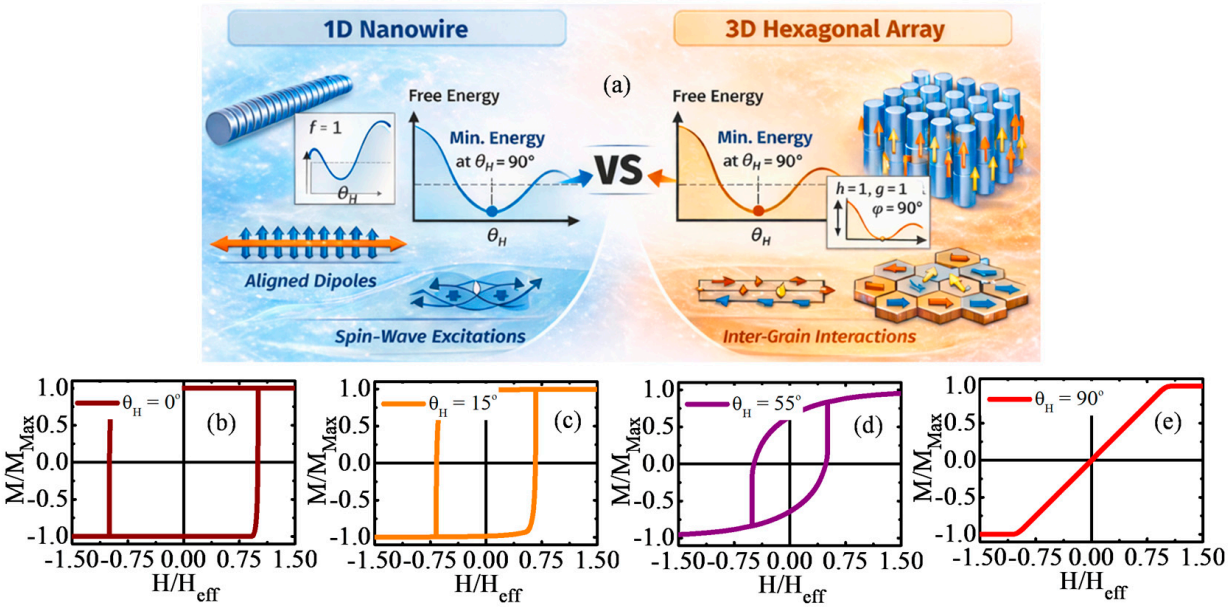

Figure 1. (**a**) Schematic illustration of magnetic energy confinement in one-dimensional (**left**) and three-dimensional (**right**) nonowire systems. A one-dimensional nanowire composed of interacting grains is shown along with the angular dependence of the free-energy density highlighting a minimum-energy state at $\theta_H = 90°$ for $f = 1$, associated with aligned dipoles and spin-wave excitations.A three-dimensional hexagonal array of nanowires, in which inter-grain dipolar and exchange interactions modify the free-energy landscape, also leading to a minimum at $\theta_H = 90°$ for $h = 1$ and $g = 1$. This comparison emphasizes how dimensionality and packing effects enable control of magnetic energy confinement, with direct implications for spin-wave dynamics and spintronic applications. (**b**–**e**) The corresponding hysteresis curves for the nanowire, highlighting its magnetic properties and behavior for four different θ_H as indicated. See text for details.

In Equation (7), the first term represents the energy density associated with dipolar interactions between grains, the second term corresponds to the demagnetizing energy density, and the last term represents the Zeeman energy density. Additionally, $\varphi = \theta - \theta_H$ is the angle between the magnetization and the applied magnetic field. Here, M_{Max} denotes the maximum magnetization in the presence of a magnetic field, r denotes the maximum magnetization in the presence of a magnetic field, $N_{//}$ is the demagnetizing factor corresponding to the longitudinal axis of the grains in the chain, V_e is the volume

of each grain, and k_n is defined as the summation $k_n = \sum_{j=1}^{n} (n-j)/nj^3$, which includes combinations for magnetic inter-grain interactions. which accounts for magnetic inter-grain interactions. In this summation, n represents the total number of grains forming the nanowire, while j denotes the number of grain pairs that are equidistant. Equation (7) can be rewritten:

$$\varepsilon_{NW} = \frac{1}{2}\sin^2(\varphi + \theta_H) - f\cos(\varphi). \quad (8)$$

The factor f is often introduced defined as $f = H/H_{eff}$, where $H_{eff} = 2\pi M_{Max}\left[1 + 3\left(V_e k_n/\pi r^3 - N_{//}\right)\right]$ and $\varepsilon_{NW} = E_{NW}/M_{Max}H_{eff}$. According to Equation (8), the magnetization component aligned with the applied magnetic field is given by $M = M_{Max}\cos(\varphi)$. Using the principle of minimum energy, the equilibrium conditions are defined by $d\varepsilon_{NW}/d\varphi|_{\varphi=\varphi_0} = 0$ and $d^2\varepsilon_{NW}/d\varphi^2|_{\varphi=\varphi_0} \geq 0$ [19].

Magnetic interactions in nanostructured systems predominantly exhibit PID behavior [24–31], a finding that underscores their complexity and significance. Typically, the relationship between the change in magnetization, Δm, and the reduced magnetization, m_r, for systems exhibiting PID behavior is expressed as $\Delta m_i = A_i\left[m_r^i\left(m_r^i - 1\right)\right]$, where A_i are constants and m_r^i lies within the closed interval [0, 1]. In current study, the applied magnetic field is directed along the easy axis of magnetization ($\theta_H = 0°$), assuming identical grains, with $A_1 = A_2 = A_3 = \ldots = 1$ and m_r^i also confined to the interval [0, 1]. Figure 2 illustrates the Δm curves, highlighted by a hatched area that delineates the interaction region, which is defined as interactive maps. This investigation reveals a maximum intensity of demagnetizing interactions of $I_{PID}^{NW}(0) = 0.167$. An in-depth analysis of the angular dependence of these interactions is essential. As reported in Ref. [31], the experimental angular dependence of the Δm curves for PID closely follows a cosine function, reinforcing the predictability of these systems. Accordingly, this relationship can be expressed as

$$\Delta m_i = \sum_{\theta=0}^{\pi/2} B_i(m_d, m_r)\cos(\theta_H). \quad (9)$$

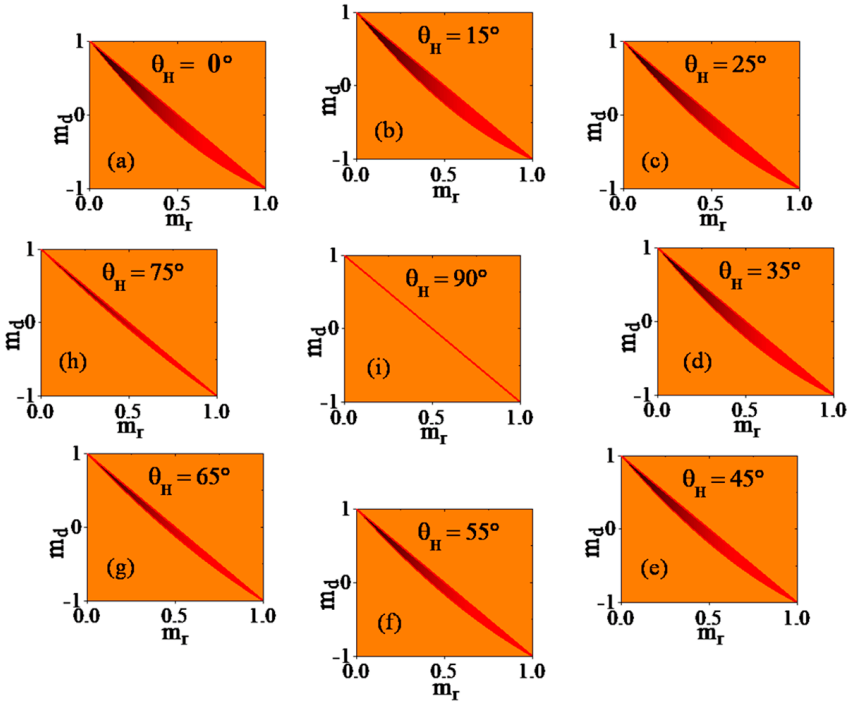

Figure 2. Δm maps of m_d as a function of m_r, for a single nanowire, calculated for various orientations θ_H of the applied magnetic field (**a**–**i**) as indicated. The hatched areas indicate regions associated with magnetic interactions. As θ_H increases toward the hard-axis orientation, the magnitude of the demagnetizing interactions progressively decreases.

In this context, $B_i(m_d, m_r)$ can be written as $A_i\left[m_r^i\left(m_r^i - 1\right)\right]$, with $A_1 = A_2 = A_3 = \ldots = 1$. Consequently, Equation (9) can be reformulated as:

$$\Delta m_i = \sum_{\theta=0}^{\pi/2}\left[m_r^i\left(m_r^i - 1\right)\right]\cos(\theta_H). \quad (10)$$

Figure 2 illustrates the maps of magnetic interactions as a function of the applied magnetic field angle, θ_H, obtained from Equations (1), (2) and (10). These interactions weaken significantly as the magnetic field approaches alignment with the hard axis of magnetization in the nanowire. This behavior highlights the strong influence of field orientation, indicating that inter-grain interactions become notably weaker when the magnetic field is perpendicular to the nanowire. Furthermore, studies of domain walls and spin-wave propagation in inter-grain regions have shown considerable promise [2,5,8,19,22]. These inter-grain domain walls are of particular interest, as they play a crucial role in the investigation of advanced magnetic systems, including skyrmions [32]. This is largely due to the well-defined nature of the domain walls in these regions, which opens compelling avenues for future research and applications in magnetic materials.

Figure 3 presents an analysis of the angular dependence of the coercivity with respect to the applied magnetic field angle, θ_H. This dependence is indicative of the coherent mode of magnetization reversal within the nanowire [1–18]. Notably, the relatively large ratio of coercivity to the effective magnetic field underscores the significance of the nanowire length in this behavior. These observations are consistent with the results shown in Figure 1b–e. By employing Equations (6) and (10), the intensity values of the PID behavior across the various interaction maps shown in Figure 2 are calculated, as presented in Figure 3b. The results demonstrate that the intensity of magnetic interactions is directly proportional to the change in magnetization, expressed as $I(\theta_H) \propto \Delta m$. For the nanowire under investigation, the angular dependence of the interaction intensity is given by $I_{PID}^{NW} = I_{PID}^{NW}(0)\cos(\theta_H)$. The excellent agreement between the numerical data shown in Figure 3 and this model yields a value of $I_{PID}^{NW}(0) = 0.167$. This relationship reinforces the understanding of magnetic interactions in nanowires and highlights their potential applications in advanced magnetic devices.

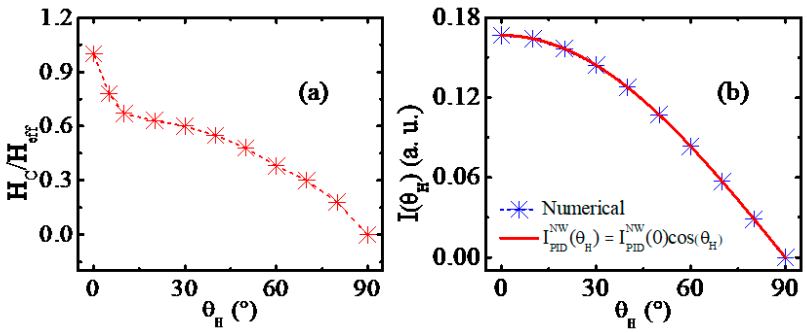

Figure 3. Nanowire data revealing key insights: (**a**) the angular dependence of the coercivity, showing how this property varies with direction and (**b**) the angular variation in the intensity $I_{PID}^{NW}(\theta_H)$, extracted from the interaction maps shown in Figure 2 and accurately described by the relation $I_{PID}^{NW} = I_{PID}^{NW}(0)\cos(\theta_H)$ $I_{PID}^{NW}(0) = 0.167$. The results underscore the critical influence of angular orientation on nanowire behavior.

3.2. 3D: Comprising a Hexagonal Array of Nanowire

The physical properties of three-dimensional materials differ from those of one-dimensional systems, such as a single nanowire. An array of nanowires may be composed of metals, semiconductors, or magnetic materials, exhibiting interactions that are unique

to their morphology [1–8]. When considering the magnetic energy density of a hexagonal array of nanowires (NWA), the total free energy density can be expressed as

$$E_{NWA} = \pi M_{Max}^2 \left[\left(\frac{3V_e k_n}{\pi r^3} \right) + (1 - 3N_{//}) - 3P \right] \sin^2(\varphi + \theta_H) - M_{Max} H \cos(\varphi) - A\cos(\varphi + \theta_H). \quad (11)$$

In Equation (11), the difference between Equations (7) and (11) corresponds to the energy density associated with the packing of nanowires in the array, given by $E_{PID}^{NWA} = -3\pi P M_{Max}^2 \sin^2(\varphi + \theta_H)$, and the exchange energy, denoted as $E_{PIM}^{Exc} = -A\cos(\varphi + \theta_H)$ [2,5,8,19,22], where P is the packing factor of the nanowires in the array and A is the exchange constant. In the context of the 3D hexagonal nanowire array considered in this approach, P represents the ratio between the volume occupied by the nanowires and the total volume of the unit cell of the array. For a hexagonal arrangement of cylindrical wires, it can be expressed geometrically as the ratio between the cross-sectional area of the wire and the area of the corresponding hexagonal lattice cell. Thus, P depends directly on the wire diameter and the distance between the centers of the nanowires. Equation (11) can be rewritten as

$$\varepsilon_{NWA} = \frac{1}{2} \sin^2(\varphi + \theta_H) - h\cos(\varphi) - gg\cos(\varphi + \theta_H). \quad (12)$$

The factors $h = H/H'_{eff}$ and $g = A/M_{Max}H'_{eff}$ are introduced to incorporate the effective field term $H'_{eff} = 2\pi M_{Max}\left[1 + 3\left(V_e k_n/\pi r^3 - N_{//} - P\right)\right]$, and $\varepsilon_{NWA} = E_{NWA}/M_{Max}H'_{eff}$. The hysteresis curves calculated using the minimum-energy conditions discussed above are shown in Figure 4. The energy densities associated with nanowire packing in the array and with exchange interactions give rise to PID and PIM behaviors, respectively. The exchange interactions are primarily influenced by defects arising from the packing of the nanowires within the array. In this context, it is necessary to include the defect term $D_i(m_d, m_r)\sin(\theta_H)$ in Equation (9) to derive the magnetic interactions for a hexagonal array of nanowires:

$$\Delta m_i = \sum_{\theta=0}^{\pi/2} [B_i(m_d, m_r)\cos(\theta_H) + D_i(m_d, m_r)\sin(\theta_H)]. \quad (13)$$

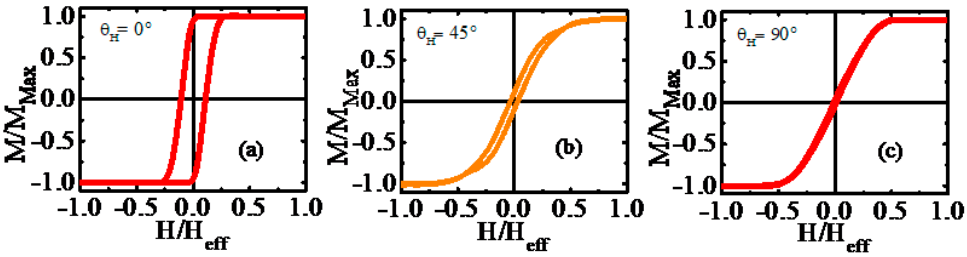

Figure 4. The hysteresis curves for the hexagonal array of nanowires, highlighting its distinctive magnetic properties and behavior for various θ_H (**a**–**c**), as indicated.

The term $D_i(m_d, m_r)$ is defined as $-m_r^2(m_r - 1)/2$, representing the average contribution of PID and PIM interactions within the array. Accordingly, Equation (13) can be rewritten as:

$$\Delta m_i = \sum_{\theta=0}^{\pi/2} \left[m_r^i \left(m_r^i - 1 \right) \right] \cos(\theta_H) - \left[\frac{(m_r^i)^2}{2} \left(m_r^i - 1 \right) \right] \sin(\theta_H). \quad (14)$$

Figure 5 presents maps of magnetic interactions at various angles of the applied magnetic field, calculated using Equations (1), (2) and (14). Consistent with the behavior observed in single nanowires, the magnetic interactions decrease as the applied magnetic

field approaches alignment with the hard axis of magnetization in the hexagonal array of nanowires. Notably, the PID decreases sharply with increasing field angle, while the PIM increases simultaneously. This behavior arises from the unique coupling between spins within the three-dimensional nanostructure, which plays a crucial role in the excitations generated by dipolar and exchange spin waves. These results highlight the complex nature of magnetic interactions in nanostructured systems and their importance for understanding nanoscale magnetic behavior.

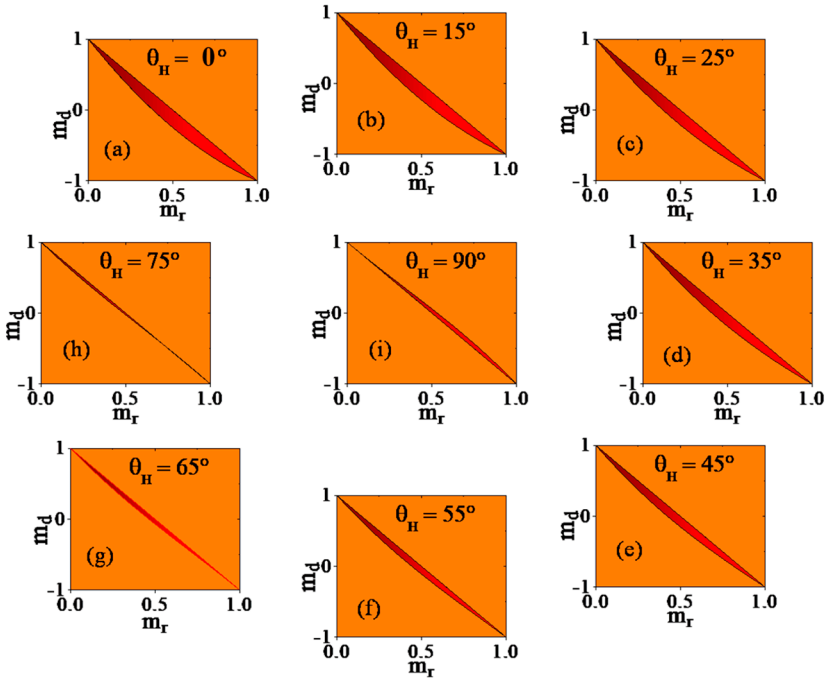

Figure 5. Δm maps of m_d as a function of m_r, for a hexagonal array of nanowire, calculated for different orientations θ_H of the applied magnetic field (**a**–**i**) as indicated. The hatched areas indicate regions associated with magnetic interactions. As θ_H increases toward the hard-axis orientation, the magnitude of the demagnetizing interactions progressively decreases.

It is crucial to account for the energy density arising from the arrangement of nanowires within the array when performing a comprehensive analytical analysis of the angular variation based on the intensity derived from PID behavior. The intensity of the PID behavior for a hexagonal array of nanowires can be expressed as

$$I_{PID} = I_{PID}^{NW}(0)\cos(\theta_H) + I_{PID}^{NWA}\sin^2(\varphi + \theta_H). \quad (15)$$

Conversely, the angular variation in the intensity associated with PIM behavior is given by

$$I_{PIM} = I_{PIM}^{NWA}(0)\cos(\varphi + \theta_H). \quad (16)$$

Equations (15) and (16) provide a robust framework for independently evaluating the intensity of magnetic interactions, a factor that is critically relevant to spin-wave propagation [8,33]. Figure 6a presents the angular dependence of the coercivity as a function of the applied magnetic field angle, θ_H. This dependence reflects the various modes of magnetization reversal occurring in the hexagonal array of nanowires. Notably, the relatively small ratio of coercivity to the effective magnetic field highlights the unique three-dimensional structure of the array, consistent with the behavior shown in Figure 4b,c. By applying Equations (6) and (14), the PID and PIM behaviors for the different interaction maps shown in Figure 5 are calculated, as presented in Figure 6b. This comprehensive analysis en-

hances the understanding of the system and highlights important implications for future research in this field. It is important to clarify that the defect term introduced for the 3D hexagonal arrangement does not derive from a complete sum of the micromagnetic lattice. Instead, it represents an effective contribution that captures the average magnetization and demagnetization interactions induced by packing in the hexagonal geometry. This term reflects the influence of lattice symmetry and local disorder on the internal field distribution. As real systems deviate from ideal periodicity, the interaction landscape is modified by symmetry-breaking effects and structural imperfections. Therefore, the defect term should be understood as a phenomenological correction intended to better describe this type of structure, and not as a rigorous quantity derived from the lattice.

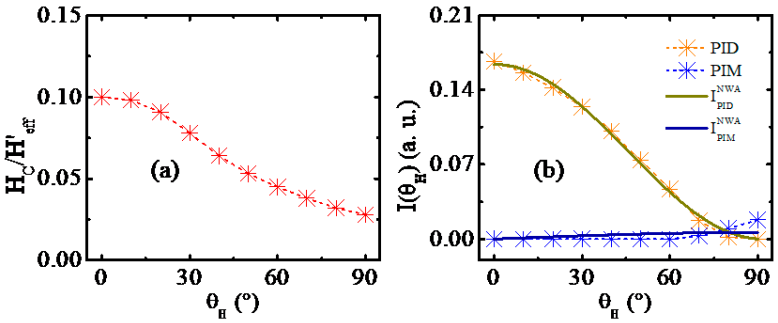

Figure 6. Hexagonal array of nanowires revealling key insights: (**a**) the angular dependence of the coercivity, showing its variation with the applied field angle. and (**b**) the angular profile of the intensity $I^{NW}_{PID}(\theta_H)$, extracted from the interaction maps shown in Figure 5, highlighting the underlying magnetic interactions in the system.

The Δm formalism employed in current study not to be interpreted as a microscopic theory of magnetic interactions, but rather as a quantitative diagnostic method originally proposed by Otto Henkel to evaluate interaction effects through IRM and DCD measurements [24]. In the present framework, Δm analysis is incorporated into an energy-based description to provide a measurable interaction-intensity parameter that reflects the balance between magnetizing and demagnetizing contributions. Its validity requires that the system operates in a quasi-static regime, where the remanent states correspond to stable or metastable energy minimum and thermal activation does not dominate the reversal process. Under these conditions, the Δm curve serves as a reliable indicator of collective interaction effects and enables direct comparison with experimental data obtained from structured magnetic systems such as experimentally obtained nanowire arrays [20–30].

3.3. Analyzing the Magnetic Energy Confinement in 1D and 3D Systems

Figure 7 illustrates the behavior of the free energy densities for both a single nanowire and a hexagonal array of nanowires. In Figure 7a, the critical conditions leading to energy minima are presented, and the inset shows how the energy varies with the direction of the applied magnetic field, specifically for f = 1, and φ = –90°. Notably, at φ = –90° and θ_H = 90°, the free energy reaches its minimum value. Figure 7b further illustrates the different conditions for energy minima as a function of the applied magnetic field orientation. The inset confirms that when h = 1, g = 1, and φ = –90°, the free energy is minimized at θ_H = 90°. Moreover, Figure 7 highlights the critical equilibrium condition of magnetization during magnetic interaction measurements, revealing the potential for spin-wave generation during equilibrium precession.

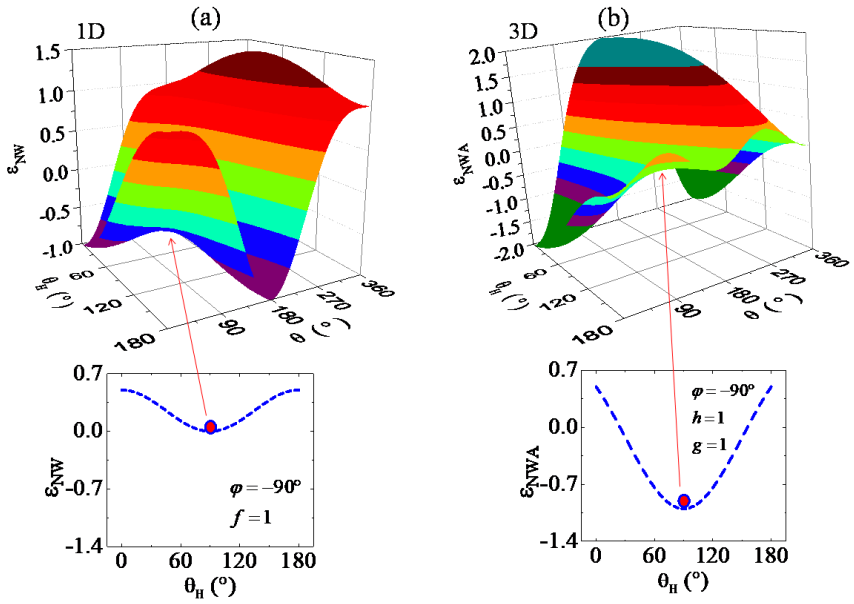

Figure 7. (**a**) The positions of minimum energy are found to be located along the nanowire axis. The zoom highlights the variation in the energy with the direction of the applied magnetic field for $f = 1$ and $\varphi = -90°$. (**b**) The hexagonal array of nanowires exhibits the same behavior as for nanowire (**a**), with the minimum energy positions also aligned along the nanowire axis. The zoom illustrates the energy variation with the applied magnetic field direction for $h = 1$, $g = 1$, and $\varphi = -90°$. In both cases (1D and 3D nanowires), the energy reaches its minimum at $\theta_H = 90°$, demonstrating the consistency of this behavior The colors indicate the levels of confinement.

Before concluding, it is worth to emphasize that the central objective of this study was to provide a physically transparent and quantitatively consistent framework for analyzing interaction effects in structured magnetic systems. Combining energy-based modeling with Δm analysis, a direct connection was established between geometric parameters such as packing factor, aspect ratio, and element spacing and measurable magnetic response functions. This approach allowed the author to isolate the respective roles of dipolar and exchange contributions and define an interaction intensity metric that can be systematically compared across different field configurations and orientations. In this context, the importance of the proposed framework lies in its balance between analytical tractability and physical interpretability. Instead of relying exclusively on complete micromagnetic simulations or purely phenomenological descriptions, a reduced model was adopted that captures the dominant mechanisms governing collective behavior while explicitly stating its assumptions and limits of applicability. In this way, the paper offers not only theoretical insight but also a practical diagnostic tool for interpreting experimental data on nanowire arrays and related particulate magnetic systems.

Finally, this paper is directly related to experimental systems, as reported in Refs. [2,11,12], and more recently in Refs. [34,35]. In these studies, the analyses are based on IRM/DCD measurements of magnetic interactions in nanowire arrays electrodeposited in porous alumina membranes, demonstrating that Δm analysis can qualitatively distinguish between magnetizing and demagnetizing regimes in structured assemblies. These experimental results highlight the importance of developing a quantitative framework capable of going beyond qualitative classification. In this context, the present model does not attempt to reproduce a specific experiment, but instead provides a complementary analytical tool for extracting a consistent interaction-intensity metric that can be directly compared with IRM/DCD data from real nanostructured systems. By enabling a systematic quantification of interaction strength in both one-dimensional chains and three-dimensional hexagonal arrays, the framework directly supports the central objective expressed in the title of

this paper—"Controlling Magnetic Energy Confinement in One- and Three-Dimensional Systems"—since tuning interaction intensity is the fundamental mechanism through which magnetic energy confinement can be engineered in structured assemblies.

4. Conclusions

According to the magnetic domain mechanism, nanoparticles can be regarded as exemplary single-domain structures. When grains are arranged linearly, they form networks of dipole moments, with nanowires representing a highly organized nanostructure. This organization enhances the potential for innovative applications in the systems under investigation. This study provides a framework for calculating relevant parameters and analyzing interaction intensities in magnetic nanostructures, making a significant contribution to the field, particularly to the understanding of magnetic energy confinement in one- and three-dimensional systems. The results obtained here demonstrate the influence of these interactions on spin-wave excitations, thereby advancing the physical understanding of interaction dynamics in nanostructures. Ultimately, this approach may accelerate the development of spintronic devices by exploiting inter-grain interactions and enabling new technological advances.

Funding: This research was supported by Conselho Nacional de Desenvolvimento Científico e Tecnológico (CNPq) with Grant Number: 300631/2025-1, Coordenação de Aperfeiçoamento de Pessoal de Nível Superior (CAPES) with grant number: PROAP2025UFRPE, and Fundação de Amparo à Ciência e Tecnologia do Estado de Pernambuco (FACEPE) with grant number: APQ-1397-3.04/24.

Data Availability Statement: Data will be made available on reasonable request.

Conflicts of Interest: The author declares no conflicts of interest.

References

1. Cvelbar, U. Large-scale synthesis of nanowires. *J. Phys. D Appl. Phys.* **2011**, *44*, 174014. [CrossRef]
2. França, C.A.; Guerra, Y.; Valadão, D.R.B.; Holanda, J.; Padrón-Hernández, E. Transmission electron microscopy as a realistic data source for the micromagnetic simulation of polycrystalline nickel nanowires. *Comput. Mater. Sci.* **2017**, *128*, 42–44. [CrossRef]
3. Liu, L.; Diao, Y.; Xia, S.; Lu, F.; Tian, J. A first principle study on systematic stability and electronic properties of GaN nanowire surface with Cs/Li/NF_3 co-adsorption. *Appl. Surf. Sci.* **2019**, *478*, 393–397. [CrossRef]
4. Lv, Z.; Liu, L.; Zhangyang, X.; Lu, F.; Tian, J. Enhanced absorptive characteristics of GaN nanowires for ultraviolet (UV) photocathode. *Appl. Phys. A* **2020**, *126*, 152. [CrossRef]
5. Hildever, L.; Ferro, T.; Dias, A.; José, A.; Estrada, F.; Holanda, J. Detecting magneto-optical interactions in nanostructures. *J. Mater. Sci. Technol. Res.* **2024**, *11*, 68–74. [CrossRef]
6. Silva, W.W.G.; Hildever, L.M.C.S.; Santos, M.C.G.; Estrada, F.; Holanda, J. Analyzing the magnetic influence on magneto-optical interactions. *J. Supercond. Nov. Magn.* **2023**, *36*, 951–955. [CrossRef]
7. Xiong, Y.; Luo, H.; Nie, Y.; Chen, F.; Day, W.; Wang, X.; Cheng, Y.; Gong, R. Synergistic effect of silica coated porous rodlike nickel ferrite and multiwalled carbon nanotube with improved electromagnetic wave absorption performance. *J. All. Comp.* **2019**, *802*, 364–372. [CrossRef]
8. Landeros, P.; Allende, S.; Escrig, J.; Salcedo, E.; Altbir, D.; Vogel, E.E. Reversal modes in magnetic nanotubes. *Appl. Phys. Lett.* **2007**, *90*, 102501. [CrossRef]
9. Holanda, J.; Santos, O.A.; Mendes, J.B.S.; Rezende, S.M. Spin-to-charge conversion and interface-induced spin Hall magnetoresistance in yttrium iron garnet/metallic bilayers. *J. Phys. Condens. Matter* **2021**, *33*, 435803. [CrossRef]
10. Mourachkine, A.; Yazyev, O.V.; Ducat, C.; Ansermet, J.-P. Template nanowires for spintronics applications: Nanomagnet microwave resonators functioning in zero applied magnetic field. *Nano Lett.* **2008**, *8*, 3683–3687. [CrossRef]
11. Yalçın, O.; Kartopu, G.; Çetin, H.; Demiray, A.S.; Kazan, S. A comparison of the magnetic properties of Ni and Co nanowires deposited in different templates and on different substrates. *J. Magn. Magn. Mater.* **2015**, *373*, 207–212. [CrossRef]
12. Bran, C.; Espejo, A.P.; Palmero, E.M.; Escrig, J.; Vázquez, M. Angular dependence of coercivity with temperature in Co-based nanowires. *J. Magn. Magn. Mater.* **2015**, *396*, 327–332. [CrossRef]
13. Castillo-Sepúlveda, S.; Corona, R.M.; Altbir, D.; Escrig, J. Magnetic properties of mosaic nanocomposites composed of nickel and cobalt nanowires. *J. Magn. Magn. Mater.* **2016**, *416*, 325–328. [CrossRef]

14. Cornejo, D.R.; Padrón-Hernández, E. Study of magnetization process in ordered Fe nanowire arrays. *J. Magn. Magn. Mater.* **2007**, *316*, E48–E51. [CrossRef]
15. Holanda, J. Analyzing the magnetic interactions in nanostructures that are candidates for applications in spintronics. *J. Phys. D* **2021**, *54*, 245004. [CrossRef]
16. Zafar, N.; Shamaila, S.; Sharif, R.; Wali, H.; Naseem, S.; Riaz, S.; Khaleeq-Ur-Rahman, M. Effects of pH on the crystallographic structure and magnetic properties of electrodeposited cobalt nanowires. *J. Magn. Magn. Mater.* **2015**, *377*, 215–219. [CrossRef]
17. Bran, C.; Fernandez-Roldan, J.A.; Palmero, E.M.; Berganza, E.; Guzman, J.; del Real, R.P.; Asenjo, A.; Fraile-Rodríguez, A.; Foerster, M.; Aballe, L.; et al. Direct observation of transverse and vortex metastable magnetic domains in cylindrical nanowires. *Phys. Rev. B* **2017**, *96*, 125415. [CrossRef]
18. García, J.; Prida, V.M.; Vivas, L.G.; Hernando, B.; Barriga-Castro, E.D.; Mendoza-Reséndez, R.; Luna, C.; Escrig, J.; Vázquez, M. Magnetization reversal dependence on effective magnetic anisotropy in electroplated Co–Cu nanowire arrays. *J. Mater. Chem. C* **2015**, *3*, 4688–4697. [CrossRef]
19. Chuev, M.A. Generalized Stoner–Wohlfarth approach and the non-Langevin magnetism of single-domain particles. *Pis'ma ZhETF* **2007**, *85*, 744–750, English translation: *JETP Lett.* **2007**, *85*, 611–616. [CrossRef]
20. Aharoni, A.; Shtrikman, S. Magnetization curve of the infinite cylinder. *Phys. Rev.* **1958**, *109*, 1522–1528. [CrossRef]
21. Aharoni, A. Angular dependence of nucleation by curling in a prolate spheroid. *J. Appl. Phys.* **1997**, *82*, 1281–1287. [CrossRef]
22. Lavín, R.; Denardin, J.C.; Escrig, J.; Altbir, D.; Cortés, A.; Gómez, H. Angular dependence of magnetic properties in Ni nanowire arrays. *J. Appl. Phys.* **2009**, *106*, 103903. [CrossRef]
23. Dong, J.; Zhang, Y.; Zhang, X.; Zhao, C.; Liu, Q.; Wang, J. Influence of tensile stress on giant magnetoimpedance effect of electroplated Ni_{1-x} Co_x/Cu composite wires. *J. All. Comp.* **2014**, *616*, 426–429. [CrossRef]
24. Henkel, O. Remanenzverhalten und wechselwirkungen in hartmagnetischen teilchenkollektiven. *Phys. Status Solidi b/Basic Sol. State Phys.* **1964**, *7*, 919–929. [CrossRef]
25. Kelly, P.E.; O'Gray, K.; Mayo, P.I.; Chantrell, R.W. Switching mechanisms in cobalt-phosphorus thin films. *IEEE Trans. Magn.* **1989**, *25*, 3881–3883. [CrossRef]
26. Klik, I.; Yao, Y.D.; Chang, C.R. Henkel plots for thermally relaxing systems. *J. Appl. Phys.* **1997**, *81*, 5230–5232. [CrossRef]
27. Mayo, P.I.; O'gRady, K.; Kelly, P.E.; Cambridge, J.; Sanders, I.L.; Yogi, T.; Chantrell, R.W. A magnetic evaluation of interaction and noise characteristics of CoNiCr thin films. *J. Appl. Phys.* **1991**, *69*, 4733–4735. [CrossRef]
28. Buehler, C.J.; Mayergoyz, I.D. Henkel plots and the Preisach approach of hysteresis. *J. Appl. Phys.* **1996**, *79*, 5746–5748. [CrossRef]
29. Wohlfarth, E.P. Relations between different modes of acquisition of the emanent magnetization of ferromagnetic particles. *J. Appl. Phys.* **1958**, *29*, 595–596. [CrossRef]
30. Grimsditch, M.; Jaccard, Y.; Schuller, I.K. Magnetic anisotropies in dot arrays: Shape anisotropy versus coupling. *Phys. Rev. B* **1998**, *58*, 539–543. [CrossRef]
31. Encinas-Oropesa, A.; Demand, M.; Piraux, L.; Huynen, I.; Ebels, U. Dipolar interactions in arrays of nickel nanowires studied by ferromagnetic resonance. *Phys. Rev. B* **2001**, *63*, 105515. [CrossRef]
32. Jiang, W.; Upadhyaya, P.; Zhang, W.; Yu, G.; Jungfleisch, M.B.; Fradin, F.Y.; Pearson, J.E.; Tserkovnyak, Y.; Wang, K.L.; Heinonen, O.; et al. Blowing magnetic skyrmion bubbles. *Science* **2015**, *349*, 283–286. [CrossRef]
33. Holanda, J.; Maior, D.S.; Azevedo, A.; Rezende, S.M. Detecting the phonon spin in magnon–phonon conversion experiments. *Nat. Phys.* **2018**, *14*, 500–506. [CrossRef]
34. Silva, W.W.G.; Dias, A.d.A.; Rodrigues, A.R.; Chávez, F.E.; de Oliveira, R.A.; Holanda, J. An experimental analysis from the magnetic interactions in nanowire arrays. *Appl. Nanosci.* **2023**, *13*, 5559–5562. [CrossRef]
35. Hildever, L.; Ferro, T.; Estrada, F.; Holanda, J. Exploring the effects of ultraviolet radiation on the properties of Fe_3O_4/PANI nanostructures. *Next Mater.* **2024**, *4*, 100209. [CrossRef]

Disclaimer/Publisher's Note: The statements, opinions and data contained in all publications are solely those of the individual author(s) and contributor(s) and not of MDPI and/or the editor(s). MDPI and/or the editor(s) disclaim responsibility for any injury to people or property resulting from any ideas, methods, instructions or products referred to in the content.